3D Kinematic Mandible Model to Design Mandibular Advancement Devices for the Treatment of Obstructive Sleep Apnea

M. García[1]; J.A. Cabrera[1]; A. Bataller[1]; S. Postigo[1]; J.J. Castillo[1].
[1]Department of Mechanical Engineering. University of Málaga. C/ Doctor Ortiz Ramos s/n
Ampliación Campus Teatinos. 29071 Málaga. Spain

Abstract
Mandibular Advancement Devices (MADs) are one of the treatments used for Obstructive Sleep Apnea (OSA). MADs try to maintain the mandible in an advanced position to keep the upper airways open when sleeping. To achieve this goal, most current MADs limit the mouth opening to a few millimetres. The study of the kinematic behaviour of the patient's jaw is essential in order to design devices that allow greater aperture ranges. For this purpose, a 3D multibody model that reproduces jaw movement has been developed in this work. To this end, the movement of the lower incisor has been determined by means of a vision system and reflective markers. In addition, the kinematics of the temporomandibular joint has been modelled. Next, the device is designed and printed using a cam-follower mechanism. This way, the cam profiles and the followers are optimally designed and positioned for each patient depending on the physiognomy of the jaw and the opening and advancing movement prescribed by the specialist.

Keywords
Mandibular advancement device, 3D Mandible kinematics, Cam-follower mechanism, 3D printed devices

1.-Introduction

Sleep apnea is a serious disorder in which patients stop breathing for short periods of time when they are asleep [1, 2]. This disorder leads to fatigue and sleepiness during the day and it is also associated to a higher risk of developing cardiovascular problems such as arrhythmias, strokes and heart attacks [3-5].

The most common type of sleep apnea is the Obstructive Sleep Apnea (OSA). OSA is a chronic disease in which the upper airway is repeatedly, partially or completely obstructed while sleeping. This disorder requires treatment in order to alleviate its effects [6]. The main existing treatments are Continuous Positive Air Pressure (CPAP), Oral Appliances (OA) and surgery. CPAP is a machine connected to the patient while sleeping that maintains a positive air pressure in the upper airways by means of a face mask. The main problems reported by patients are related to the noise produced by the machine and the excessive dryness of the upper airways. An alternative to CPAP are the Mandibular Advancement Devices (MADs), which are a type of OA [7]. MADs are designed to keep the mandible in an advanced position so that the upper airway is open and does not collapse when the patient sleeps [2, 8, 9]. These devices are composed of two pieces that fit into the dental arches and force the jaw to remain in a protruded position [10-11]. Compared to CPAP, MADs are not noisy and they are much more economical, easy to use and do not require a power system.

There is currently a wide variety of MAD models, with different strategies to keep the jaw in an advanced position [12]. Several methods are used to connect the two pieces that compose a MAD. These methods include the use of bars, elastic straps, springs, telescopic rods, tube connectors and lateral fins among others [13]. The use of this type of mechanism reduces the degrees of freedom of the jaw and limits mouth opening and lateral motion. However, users prefer models that allow wider ranges of mouth opening and lateral movement of the jaw. Another valued feature is maximum space for the tongue and no metallic parts. In this sense, devices using lateral fins (cams) are reported to be more comfortable. On one hand, there are no moving elements, such as bars or springs and, on the other hand, there are no metal parts in contact with the tongue. In addition, devices based on the use of cams can be designed to allow lateral movement of the jaw. All these devices do not take into account the kinematics of the patient's mandible. Therefore, the movement of the jaw when the device is used is not known a priori and may cause the device to lose effectiveness when the patient opens the mouth.

For this reason, the study of the patient's jaw movement is required to design customized devices. Research works related to the kinematic and dynamic behaviour of the jaw can be found in [14-15]. These works focus on the behaviour of the jaw in mastication processes. Similarly, several robots that try to imitate jaw movements in chewing have been studied [16-19]. These results are used to propose rehabilitation methods and to study the behaviour of muscles and forces involved in mastication processes.

Biomimetic engineering can be used for the development of these robots and mechanisms. This way, the movement of the jaw is studied and recorded. Next, these devices are designed to reproduce this movement as faithfully as possible. Related to this, there are works that measure the movements of the mandible. One of the first researchers to study the jaw kinematics was Posselt in [20], where the border movements in the sagittal, frontal and lateral planes of the lower incisor were described. Many research groups have tried to reproduce these diagrams using devices mounted on the dental arches [21-24]. These works have contributed to achieving a better knowledge of the movements of the jaw and, thus, a more accurate determination of its border movements. The study of mandible motion can be used to detect problems in the temporomandibular joint and establish movement patterns that help to design robots and mechanisms, among other applications.

To the best of our knowledge, only one paper has been devoted to describing a method to design personalized devices based on the use of lateral fins or cams depending on the patient's jaw kinematic [25]. Not taking into account the movement of patient's jaw can cause MADs to be ineffective when opening the mouth and poor performance which may cause the patient to drop out of treatment.

In the previous work developed by Bataller et al. [25], a kinematic model of the jaw with two degrees of freedom was described. However, only the movement in the sagittal plane was considered. This methodology yields to a symmetrical design of the cams in the MAD. As a result, the left side cam profile was exactly the same as the right side one and both cams were in the same relative position. While the proposed methodology in the cited work performed properly in most patients, it may cause the device to malfunction in patients with temporomandibular joint asymmetry and malformations. To cope with this lacks, this work has been developed to improve the design of MADs, allowing their personalization by means of a 3D kinematic model that reproduces the movement of patients' mandibles considering the two temporomandibular joints separately and their possible asymmetry.

Therefore, the aim of this study is to obtain an accurate kinematic model of the mandible and temporomandibular joint of a patient. To achieve this goal, a system that records jaw movements in 3D by means of infrared cameras and markers at different points of the mandible has been used. Once the model of the jaw has been obtained, the design of the mandibular advancement device can be carried out using two cams and two followers that are positioned laterally in the upper and lower splints. The final design guarantees that the mandible does not move backwards at any time while opening the mouth. The design also takes into account factors that help to improve the comfort level such as high lateral movement, free tongue space, non-metallic pieces and non-intrusive cam design.

Therefore, the main contributions of this paper are the following:

- To develop a 3D kinematic model of the mandibular movement.
- To detail the methodology to accurately measure the movement of the mandible using a new camera/vision-based measurement system.
- To describe the methodology to design customized mandibular advancement devices for patients with asymmetries in the jaw movement.
- To apply this new approach to a real case and compare the results obtained with a previous proposed method.

This paper has been structured as follows. In section 2, the three-dimensional system used to record jaw motion is described. Once the movement of the lower incisor has been determined, the procedure to obtain the kinematics of the temporomandibular joint is developed in section 3. Then, in section 4, natural coordinates are used to create a 3D multibody model of the mandible based on previous results. The methodology to design the mandibular advancement device personalized for each patient is also included in this section. Finally, the conclusions of this work are drawn in section 5.

2.-Three-dimensional mandibular movement recording system

Accurate measurement of the patient's jaw movement is required to properly design customized devices. In [25], a patient's scanner or X-Ray was used to measure the mandibular length, the condyle radius and the x-y coordinates of the maximum and minimum points of the articular fossa curve. The rest of the needed values, such as protrusion (Pr), retrusion (Re) and mouth opening (MO), could be measured by an orthodontist or a dentist. It has been observed that this methodology is not adequate for patients with asymmetries in the jaw movement. In these cases, it is required to determine the movement of the trajectories of both condyles. This way, a 3D Vicon system (Oxford Metrics®, Oxford, UK) with four infrared cameras was used to determine the jaw movement in this paper. To this end, two trihedrons with six markers were manufactured and inserted between the lower and upper dental arches of a patient with a splint (see Figure 1).

a) b)

Figure 1.-a) Vicom infrared camera system. b) Trihedrons with markers to record mandible movements.

The movement of the upper and lower incisor and, consequently, the border movement of the lower incisor can be obtained with this system. To do so, the specialist indicates the required movements to the patient to determine the limits of mouth opening and protrusion, retrusion and lateral movement of the mandible. All these movements are recorded by the system at a frequency of 100 Hz and subsequently processed to obtain the model of the mandibular movement. The jaw model and the markers that have been used to determine the positions of the upper and lower incisor and the right and left condyle are shown in figure 2.

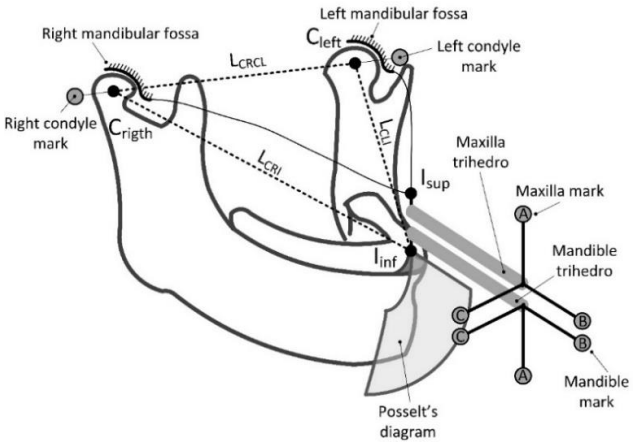

Figure 2.-3D model of the jaw with markers to determine incisor and condyle movements.

3.-Mathematical model to obtain condyle trajectories

A 3D mathematical model is required to determine the trajectories of both condyles. The use of a 2D model cannot accurately reproduce the trajectory of both condyles in case of patients with malfunctions of the jaw. This way, this section is devoted to describing a procedure to obtain the movement of the incisors and condyles using a 3D model. First, the position of two reference points on the lower and upper incisor (I_{sup} and I_{inf}) are obtained from the coordinates of each of the trihedron marks (A, B and C) during the prescribed movements (see figure 3).

Once the positions of each of the trihedron marks of the mandible and maxilla have been measured, the position of the lower and upper incisor can be obtained at each instant. In addition, the rest position of the right and left condyle can also be obtained. To do so, two markers are placed on the outer part of each condyle. Knowing the position of the condyle with respect to the mark, the distance between the two condyles (L_{CRCL}) and the distances from them to the reference point of the lower incisor (L_{CRI} and L_{CLI}) are determined by conducting a stationary test in the resting position of the jaw. The accuracy of these values depends on the correct positioning of the condyle mark.

These distances can also be measured on an x-ray or scan of the patient. This way, the positions of the lower incisor and right and left condyle with respect to a reference system fixed to the upper incisor are obtained (see figure 4). This method allows a direct and accurate measurement of L_{CRCL}, L_{CRI} and L_{CLI} lengths. However, the main disadvantage is that the patient needs to be x-rayed.

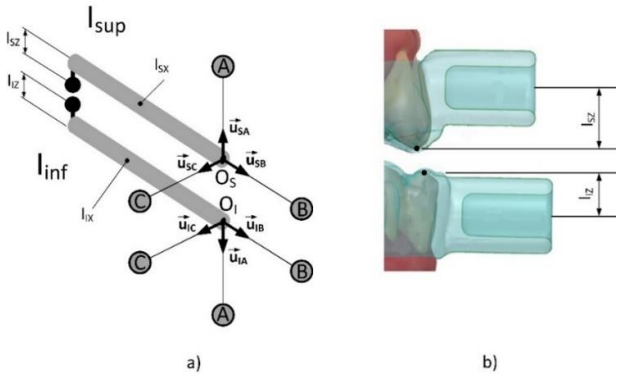

Figure 3.-Upper and lower trihedrons joined respectively to the upper and lower incisors. a) Trihedron model. b) Detail of the joining between the splints and the incisors.

The first step is to obtain the position of the origin of the coordinate system defined by the lower and upper trihedrons, O_I and O_S respectively. To this end, the following system of equations has been used:

$$\bar{u}_{SB} \times \bar{u}_{SA} = \bar{u}_{SC} \quad (1)$$

$$\bar{u}_{IA} \times \bar{u}_{IB} = \bar{u}_{IC} \quad (2)$$

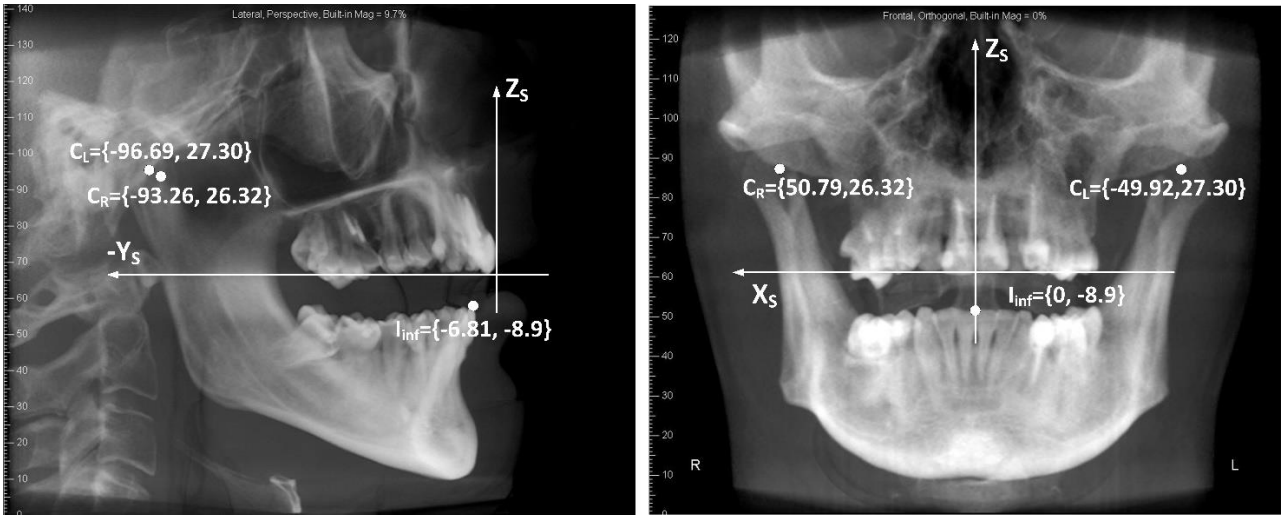

Figure 4.-Lateral and frontal X-ray of the patient with coordinates of the points of interest.

Where:

$$\bar{u}_{SA} = \frac{1}{l_T} \cdot \begin{bmatrix} x_{SA} - x_{OS} \\ y_{SA} - y_{OS} \\ z_{SA} - z_{OS} \end{bmatrix} \quad \bar{u}_{SB} = \frac{1}{l_T} \cdot \begin{bmatrix} x_{SB} - x_{OS} \\ y_{SB} - y_{OS} \\ z_{SB} - z_{OS} \end{bmatrix}$$
$$\bar{u}_{SC} = \frac{1}{l_T} \cdot \begin{bmatrix} x_{SC} - x_{OS} \\ y_{SC} - y_{OS} \\ z_{SC} - z_{OS} \end{bmatrix} \quad (3)$$

$$\bar{u}_{IA} = \frac{1}{l_T} \cdot \begin{bmatrix} x_{IA} - x_{OI} \\ y_{IA} - y_{OI} \\ z_{IA} - z_{OI} \end{bmatrix} \quad \bar{u}_{IB} = \frac{1}{l_T} \cdot \begin{bmatrix} x_{IB} - x_{OI} \\ y_{IB} - y_{OI} \\ z_{IB} - z_{OI} \end{bmatrix}$$
$$\bar{u}_{IC} = \frac{1}{l_T} \cdot \begin{bmatrix} x_{IC} - x_{OI} \\ y_{IC} - y_{OI} \\ z_{IC} - z_{OI} \end{bmatrix} \quad (4)$$

Where l_T is the distance between the origin of the coordinate system and the markers of each trihedron. From the positions of reference points A, [(x_{IA}, y_{IA}, z_{IA}), (x_{SA},y_{SA},z_{SA})], B , [(x_{IB}, y_{IB}, z_{IB}), (x_{SB},y_{SB},z_{SB})] and C, [(x_{IC}, y_{IC}, z_{IC}), (x_{SC},y_{SC},z_{SC})], the coordinates of points O_I (x_{OI}, y_{OI}, z_{OI}) and O_S (x_{OS}, y_{OS}, z_{OS}) can be obtained using equations (1) and (2).

Once the locations of the trihedron origins are known, the coordinates of the upper and lower incisors (I_{inf}, I_{sup}) in the global reference system can be calculated from equations (5) and (6), (see Figure 6):

$$I^0_{inf} = \begin{bmatrix} x_{I_i} \\ y_{I_i} \\ z_{I_i} \end{bmatrix}^0 = \begin{bmatrix} x_{OI} \\ y_{OI} \\ z_{OI} \end{bmatrix} - l_{IX} \cdot \begin{bmatrix} u^x_{IB} \\ u^y_{IB} \\ u^z_{IB} \end{bmatrix} - l_{IZ} \cdot \begin{bmatrix} u^x_{IA} \\ u^y_{IA} \\ u^z_{IA} \end{bmatrix} \quad (5)$$

$$I^0_{sup} = \begin{bmatrix} x_{I_s} \\ y_{I_s} \\ z_{I_s} \end{bmatrix}^0 = \begin{bmatrix} x_{OS} \\ y_{OS} \\ z_{OS} \end{bmatrix} - l_{SX} \cdot \begin{bmatrix} u^x_{SB} \\ u^y_{SB} \\ u^z_{SB} \end{bmatrix} - l_{SZ} \cdot \begin{bmatrix} u^x_{SA} \\ u^y_{SA} \\ u^z_{SA} \end{bmatrix} \quad (6)$$

Where distances l_{IX}, l_{SX}, l_{IZ} y l_{SZ} are defined in Figure 4. Next, the model shown in figure 5 is used to obtain the movement of the condyles.

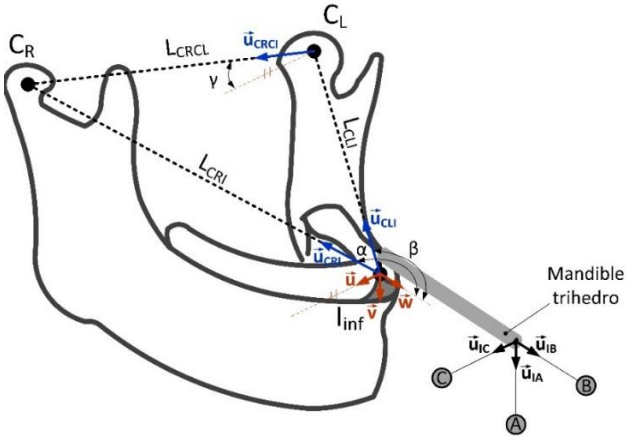

Figure 3.-Model of the jaw to obtain coordinates of the condyle

In this model, the coordinates of the lower incisor in the reference system linked to the upper incisor $I^S_{inf} = \{x_{I_i}, y_{I_i}, z_{I_i}\}$ and the unit vectors $\vec{w}$ and $\vec{u}$, parallel to the trihedron vectors $\vec{u}_{IB}$ and $\vec{u}_{IC}$ respectively, are known. Angles α, β and γ and distances L_{CRI}, L_{CLI} and L_{CRCL} are also known, since these values can be obtained using the markers located in the condyle or using a frontal and lateral x-ray oriented in the $\vec{w}$ and $\vec{u}$ direction respectively as explained before. Therefore, the coordinates of the movement of the lower incisor are (see figure 6):

$$\vec{R}^O_I = \vec{R}^0_S + \vec{r}^0_{rel} \quad (7)$$

$$\vec{r}^0_{rel} = \vec{R}^0_I - \vec{R}^0_S = \begin{bmatrix} x_{I_i} \\ y_{I_i} \\ z_{I_i} \end{bmatrix}^0 - \begin{bmatrix} x_{I_s} \\ y_{I_s} \\ z_{I_s} \end{bmatrix}^0 \quad (8)$$

$$I^S_{inf} = \begin{bmatrix} x_{I_i} \\ y_{I_i} \\ z_{I_i} \end{bmatrix} = \vec{r}^S_{rel} = S^{S0} \cdot \vec{r}^0_{rel} \rightarrow S^{S0} = \begin{bmatrix} u^x_{SC} & u^y_{SC} & u^z_{SC} \\ u^x_{SB} & u^y_{SB} & u^z_{SB} \\ u^x_{SA} & u^y_{SA} & u^z_{SA} \end{bmatrix} \quad (9)$$

Once these data have been obtained, the following equations provide the position of the condyles with respect to the reference point of the lower incisor:

$$(x_{CR} - x_{I_i})^2 + (y_{CR} - y_{I_i})^2 + (z_{CR} - z_{I_i})^2 - L^2_{CRI} = 0 \quad (10)$$

$$(x_{CL} - x_{I_i})^2 + (y_{CL} - y_{I_i})^2 + (z_{CL} - z_{I_i})^2 - L^2_{CLI} = 0 \quad (11)$$

$$(x_{CR} - x_{CL})^2 + (y_{CR} - y_{CL})^2 + (z_{CR} - z_{CL})^2 - L^2_{CRCL} = 0 \quad (12)$$

$$(x_{I_i} - x_{CR}) \cdot w_x + (y_{I_i} - y_{CR}) \cdot w_y + (z_{I_i} - z_{CR}) \cdot w_z - L_{CRI} \cdot \cos\alpha = 0 \quad (13)$$

$$(x_{I_i} - x_{CL}) \cdot w_x + (y_{I_i} - y_{CL}) \cdot w_y + (z_{I_i} - z_{CL}) \cdot w_z - L_{CLI} \cdot \cos\beta = 0 \quad (14)$$

$$(y_{CR} - y_{CL}) \cdot u_z - (z_{CR} - z_{CL}) \cdot u_y - u_x \cdot L_{CRCI} \cdot \sin\gamma = 0 \quad (15)$$

$$(z_{CR} - z_{CL}) \cdot u_x - (x_{CR} - x_{CL}) \cdot u_z - u_y \cdot L_{CRCI} \cdot \sin\gamma = 0 \quad (16)$$

$$(x_{CR} - x_{CL}) \cdot u_y - (y_{CR} - y_{CL}) \cdot u_x - u_z \cdot L_{CRCI} \cdot \sin\gamma = 0 \quad (17)$$

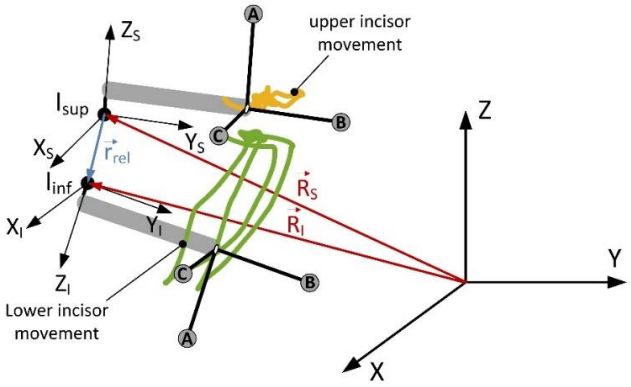

Figure 4.-Upper and lower incisive movement with respect to the absolute reference frame.

The coordinates of the condyles $C_R = \{x_{CR}, y_{CR}, z_{CR}\}$ and $C_I = \{x_{CI}, y_{CI}, z_{CI}\}$ are calculated from the previous set of equations, eqs. (10) to (17). Note that the coordinates of the position of the lower incisor used in the equations are not referred to the global system (equation (5) but to the coordinate system linked to the upper incisor. This way, it is possible to determine the movement of the jaw with respect to the maxilla even when the latter is moving (see Figure 6).

Once the coordinates of the position of the condyle with respect to the reference system linked to the upper incisor have been obtained, two third-order polynomial curves are fitted to reproduce the trajectory of the left and right condyles respectively (see Figure 7). These curves (see Figure 7b) are obtained using the patient's data shown in Table 1. It can be seen that the trajectories followed by the right and left condyles are different. While the use of a 2D jaw model perfoms well in many cases, the use of the proposed 3D model allows obtaining a more precise description of the movement of both condyles. As it is shown in figure 7b, only the trajectory of the condyle during the mouth opening and protrusion movements in Posselt's diagram has been fitted. These curves are used to design a customized MAD in the next section.

Table 1.- Patient's biometric values.

L_{CRI} [mm]	L_{CLI} [mm]	L_{CRCL} [mm]	α [deg]	β [deg]	γ [deg]
106.27	109	100.77	144.44	145.62	2.18

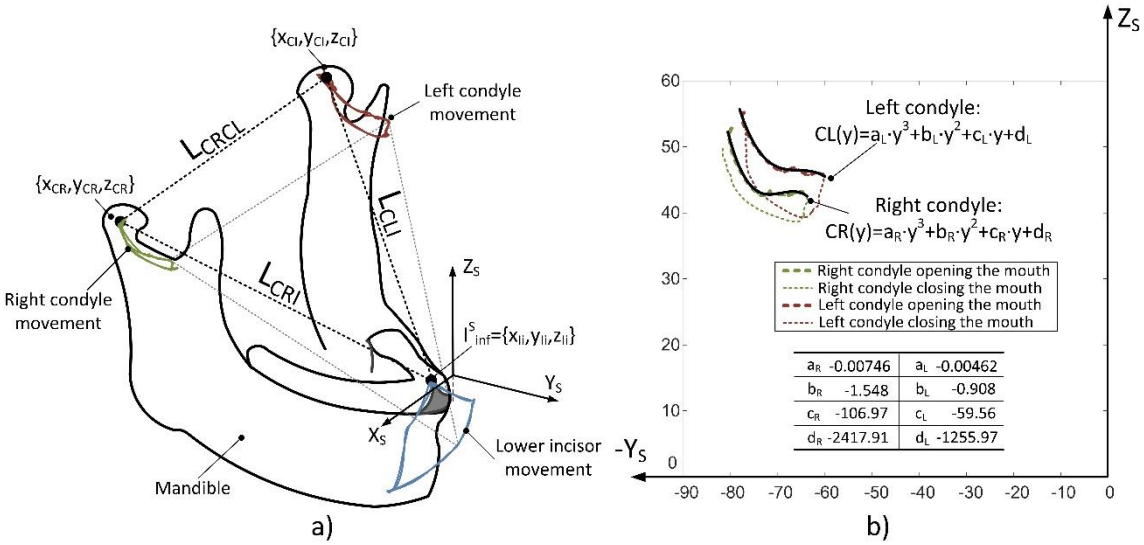

Figure 5.-Condyle movements. a) 3D model. b) Adjustment of condyle curves in the sagittal plane

4.-Design of a mandibular advancement device

Three points are defined to model the solid that reproduces the jaw. These three points are located in the condyles and in the lower incisor (see Figure 8). The reference axes are defined with the origin of the coordinate system located on the upper incisor that remains fixed to the skull. Therefore, the set of natural coordinates [26] are:

$$q = \{x_{CR}, y_{CR}, z_{CR}, x_{CL}, y_{CL}, z_{CL}, x_{I_i}, y_{I_i}, z_{I_i}\} \quad (18)$$

The joint of the condyle with the mandibular fossa is a kinematic pair with 5 dof. The movement of the condyle in a perpendicular direction to the fossa shape, due to the deformation of the joint disk, is considered negligible. Therefore, the mandible model has 4 degrees of freedom (dof). Thus, the coordinate set is not free and 5 restriction equations are introduced:

$$\left(x_{CR} - x_{I_i}\right)^2 + \left(y_{CR} - y_{I_i}\right)^2 + \left(z_{CR} - z_{I_i}\right)^2 - L_{CRI}^2 = 0 \quad (19)$$

$$\left(x_{CL} - x_{I_i}\right)^2 + \left(y_{CL} - y_{I_i}\right)^2 + \left(z_{CL} - z_{I_i}\right)^2 - L_{CLI}^2 = 0 \quad (20)$$

$$(x_{CR} - x_{CL})^2 + (y_{CR} - y_{CL})^2 + (z_{CR} - z_{CL})^2 - L_{CRCL}^2 = 0 \quad (21)$$

$$z_{CR} - (a_R \cdot y_{CR}^3 + b_R \cdot y_{CR}^2 + c_R \cdot y_{CR} + d_R) = 0 \quad (22)$$

$$z_{CL} - (a_L \cdot y_{CL}^3 + b_L \cdot y_{CL}^2 + c_L \cdot y_{CL} + d_L) = 0 \quad (23)$$

Equations (19) to (21) define the rigid solid condition of points CR, CL and I. Equations (22) and (23) set the condition for the movement of the condyles in the curves defined by the glenoid fossas. These curves were calculated in the previous section. Thus, the condyles can move on a surface where the y_{CR} and z_{CR} coordinates of the right condyle and the y_{CL} and z_{CL} coordinates of the left condyle change according to equations (22) and (23). In the case of the x_{CR} and x_{CL} coordinates, these are established by the restrictions in our model and the movement of the jaw. Therefore, a surface parallel to the Y_S Z_S plane is defined for the movement of the condyles (see Figure 8).

In order to reproduce the mandibular movement when a patient uses the MAD, 4 restrictions for the 4 dof of the jaw are introduced. In this paper, the following data are used:

- The positions of the lower incisor $I_{inf}^S = \{x_{I_i}, y_{I_i}, z_{I_i}\}$ for the correct functioning of the device when patients' open their mouth. These positions are points on the desired trajectory for the lower incisor prescribed by the specialist to ensure that the jaw is kept in a protruded position. In the example developed in this paper 9 positions have been used.
- The coordinate $\{x_{CR}\}$ of the right condyle. This restricts the lateral movement of the jaw when designing the device cams. However, this movement will be allowed in the final design of the device,

allowing patients to move their jaw laterally as we will see later.

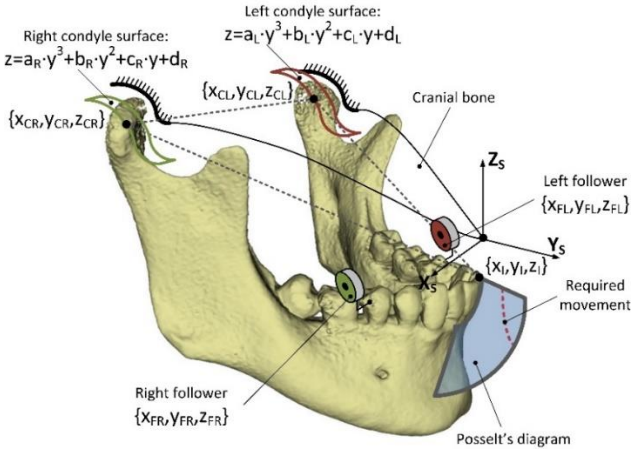

Figure 6.-Multibody model of the mandible

An iterative process is proposed to solve the kinematics of the model in equation (24):

$$\Phi_q(\boldsymbol{q}) \cdot (\boldsymbol{q}_{i+1} - \boldsymbol{q}_i) = -\Phi(\boldsymbol{q}) \quad (24)$$

where $\boldsymbol{q}$ is the set of natural coordinates defined in (18), $\Phi(\boldsymbol{q})$ is the set of constraints defined in equations (19) to (23) and $\Phi_q(\boldsymbol{q})$ is the Jacobian of the set of constraints with respect to the coordinates. Once the system (24) has been solved for all input positions, the movement of any point on the jaw can be obtained.

If the position of any singular point during jaw movement has to be known, the generalized set of coordinates has to be increased with the coordinates of that point (equation (25)). This is used to know the positions of two followers of the cams of the device (see Figure 8).

$$q = \left\{ \begin{matrix} x_{CR}, y_{CR}, z_{CR}, x_{CL}, y_{CL}, z_{CL}, x_{I_i}, y_{I_i}, z_{I_i}, x_{FR}, y_{FR}, z_{FR}, \\ x_{FL}, y_{FL}, z_{FL} \end{matrix} \right\} \quad (25)$$

$$(x_{FR} - x_{I_i}) - \alpha_{FR} \cdot (x_{CR} - x_{I_i}) - \beta_{FR} \cdot (x_{CL} - x_{I_i}) - \gamma_{FR} \cdot (x_{CR} - x_{CL}) = 0 \quad (26)$$

$$(y_{FR} - y_{I_i}) - \alpha_{FR} \cdot (y_{CR} - y_{I_i}) - \beta_{FR} \cdot (y_{CL} - y_{I_i}) - \gamma_{FR} \cdot (y_{CR} - y_{CL}) = 0 \quad (27)$$

$$(z_{FR} - z_{I_i}) - \alpha_{FR} \cdot (z_{CR} - z_{I_i}) - \beta_{FR} \cdot (z_{CL} - z_{I_i}) - \gamma_{FR} \cdot (z_{CR} - z_{CL}) = 0 \quad (28)$$

$$(x_{FL} - x_{I_i}) - \alpha_{FL} \cdot (x_{CR} - x_{I_i}) - \beta_{FL} \cdot (x_{CL} - x_{I_i}) - \gamma_{FL} \cdot (x_{CR} - x_{CL}) = 0 \quad (29)$$

$$(y_{FL} - y_{I_i}) - \alpha_{FL} \cdot (y_{CR} - y_{I_i}) - \beta_{FL} \cdot (y_{CL} - y_{I_i}) - \gamma_{FL} \cdot (y_{CR} - y_{CL}) = 0 \quad (30)$$

$$(z_{FL} - z_{I_i}) + \alpha_{FL} \cdot (z_{CR} - z_{I_i}) - \beta_{FL} \cdot (z_{CL} - z_{I_i}) - \gamma_{FR} \cdot (z_{CR} - z_{CL}) = 0 \quad (31)$$

Using equations (19) to (23) and (26) to (31), the movements of the centre of each follower are obtained and, consequently, the path they have to follow to ensure that the lower incisor moves along the trajectory established by the specialist to guarantee of the MAD.

Equations (26) to (31) provide the points of the right and left follower with respect to the base formed by points C_R, C_L and I_{inf}. Parameters α_{FR}, β_{FR}, γ_{FR}, α_{FL}, β_{FL}, and γ_{FL} are determined by the position that the designer determines to be appropriate for the followers.

Figure 9 shows the mandible movement sequence of a patient whose data are given in table 1. The data for the position of the followers and the coefficients of the condyle curves for this example are exposed in Table 2. As shown in figure 9, the cams are attached to the maxilla and the followers to the mandible in this example. This is done by means of two splints with the dental impression of the patient. The trajectories of the condyles when the lower incisor follows the nine prescribed positions are shown in Table 3.

The trajectories of the centre of the followers in the sagittal plane (y_{FR}, z_{FR}, y_{FL}, z_{FL}) are determined to design the profile of the cams, as mentioned above. Knowing the radius of the followers, the cam profiles are determined by finding the contact points in each position between the cam and the follower (see Figure 10) [25].

For the sake of clarity, only the profile of the right cam has been drawn In Figure 10. However, it has to be emphasized that the trajectories of the centre of the followers are not symmetrical with respect to the sagittal plane (see Table 4). Therefore, the position of the left cam can be different from the right one in the sagittal plane.

Table 2.-Parameters to obtain the position of the followers and the condyle curves

α_{FR}	β_{FR}	γ_{FR}	a_R	b_R	c_R	d_R
-90.0778	90.3106	90.3660	-0.00746	-1.548	-106.97	-2417.91
α_{FL}	β_{FL}	γ_{FL}	a_L	b_L	c_L	d_L
-17.2905	17.5261	17.2628	-0.00462	-0.908	-59.56	-1255.97

Table 3.-X, Y and Z coordinates of the condyles and lower incisor.

	x[mm]	y[mm]	z[mm]		x[mm]	y[mm]	z[mm]		x[mm]	y[mm]	z[mm]
I_{i1}	1.36	5.97	-3.14	C_{R1}	44.86	-76.66	45.13	C_{L1}	-55.80	-73.25	48.73
I_{i2}	-1.30	5.65	-5.55	C_{R2}	44.86	-75.98	44.44	C_{L2}	-55.79	-72.37	48.06
I_{i3}	-1.24	5.45	-7.69	C_{R3}	44.86	-75.24	43.86	C_{L3}	-55.78	-71.42	47.50
I_{i4}	-1.19	5.38	-9.65	C_{R4}	44.86	-74.38	43.37	C_{L4}	-55.77	-70.35	47.05
I_{i5}	-1.13	5.46	-11.53	C_{R5}	44.86	-73.31	43.00	C_{L5}	-55.76	-69.06	46.71
I_{i6}	-1.07	5.71	-13.43	C_{R6}	44.86	-71.88	42.81	C_{L6}	-55.75	-67.42	46.50
I_{i7}	-1.01	6.16	-15.43	C_{R7}	44.86	-69.88	42.94	C_{L7}	-55.76	-65.31	46.41
I_{i8}	-0.96	6.82	-17.63	C_{R8}	44.86	-67.27	43.24	C_{L8}	-55.78	-62.78	46.25
I_{i9}	-0.90	7.72	-20.13	C_{R9}	44.86	-64.57	42.92	C_{L9}	-55.79	-60.14	45.54

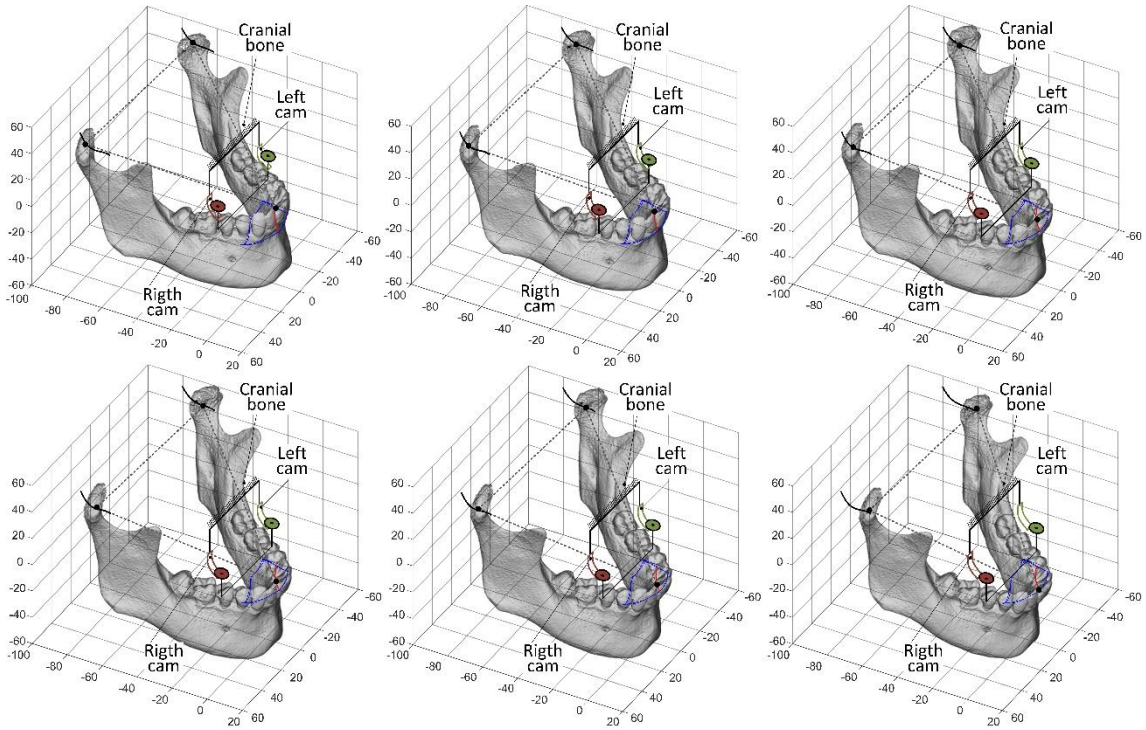

Figure 7.-Mandible movement sequence with cams and followers

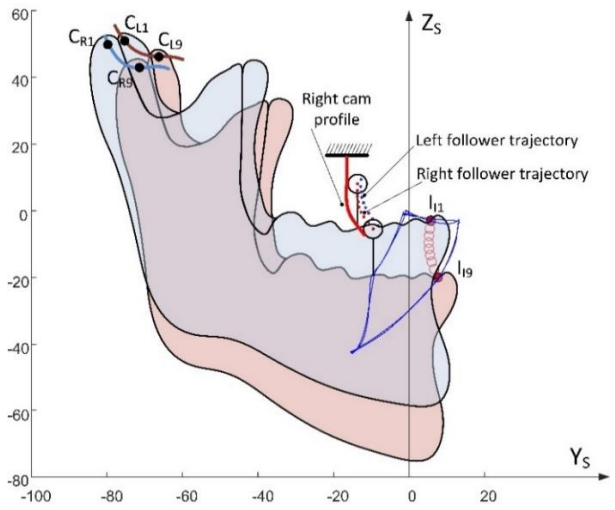

Figure 8.-Profile of the right cam linked to the maxilla.

The methodology proposed in this paper has been compared to the methodology described in [25]. To this end, two MADs have been designed. The first MAD has been obtained using the measurement system and 3D jaw model described in this paper. Next, a second MAD has been designed using the methodology explained in [25]. Figure 11 shows the result of this comparison. It can be seen that the trajectory followed by the lower incisor with the new approach allows a wider mouth opening (19.7 mm) compared to the one obtained with the previous method (11.8 mm). As expected, the cam profile obtained with the previous methodology yields to a lower incisor movement being restricted to the sagittal plane. On the contrary, the new device allows a 3D movement of the lower incisor. As we can see in figure 11, if the specialist prescribes a MAD able to provide a vertical opening of the mouth of 17 mm, the trajectory followed by the lower incisor in the 3D case is correct and the advancement when the patient opens the mouth is always positive (figure 11b). However, the advancement is negative and the device loses effectiveness when using the device designed with the 2D model.

As it has been shown, the methodology proposed in this paper can cope with irregularities in the temporomandibular joints and in the trajectory followed by the condyles. Personalized MAD's obtained with this approach have better performance compared to previous methodologies since the cam profiles in the designed devices allow a wider range of mouth opening. Thus, this methodology allows designing devices for patients with asymmetries in the jaw movement.

The final design of the device is shown in figure 12. The designed mechanism has the followers joined to the upper splint attached to the maxilla, and the cams joined to the splint attached to the mandible. It can also be seen that there is a lateral space between the upper splint and the cams, which allows lateral movement of the jaw. The device can also be designed with the cams attached to the mandible and the followers fixed to the maxilla [14].

Table 4.-X, Y and Z coordinates of the centre of the followers.

	x[mm]	y[mm]	z[mm]		x[mm]	y[mm]	z[mm]
F_{R1}	14.97	-13.46	7.90	F_{L1}	-16.97	-12.61	9.18
F_{R2}	15.02	-13.56	5.90	F_{L2}	-16.92	-12.63	7.19
F_{R3}	15.06	-13.55	4.12	F_{L3}	-16.88	-12.56	5.42
F_{R4}	15.10	-13.42	2.49	F_{L4}	-16.83	-12.36	3.82
F_{R5}	15.15	-13.12	0.96	F_{L5}	-16.79	-11.98	2.30
F_{R6}	15.19	-12.60	-0.54	F_{L6}	-16.74	-11.40	0.80
F_{R7}	15.23	-11.80	-2.03	F_{L7}	-16.70	-10.56	-0.76
F_{R8}	15.28	-10.68	-3.62	F_{L8}	-16.66	-9.46	-2.50
F_{R9}	15.32	-9.36	-5.59	F_{L9}	-16.62	-8.15	-4.60

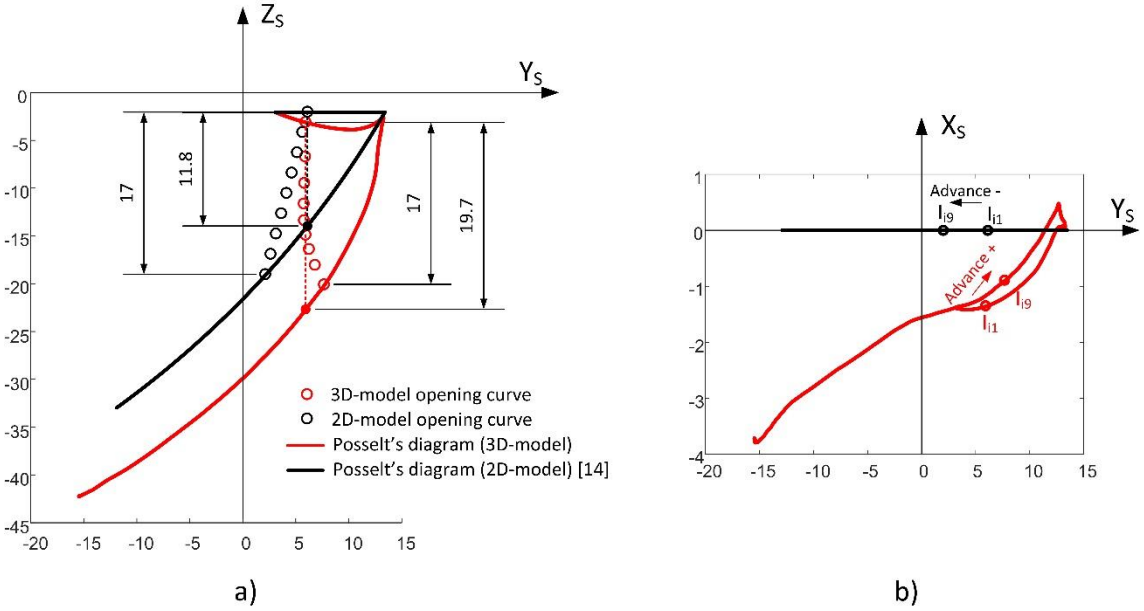

Figure 9.- 3D-model versus 2D-model comparative study. a) Posselt's diagrams in the sagittal plane. b) Posselt's diagrams in the horizontal plane.

The final device (Figure 12b) was printed in 3D using selective laser sintering technology (SLS) and biocompatible material, allowing an accurate position of the cams and followers, ensuring the correct functioning of the device and contributing to a perfect fit in the patient's dental arches.

Figure 10.-Final design of MAD. a) CAD/CAM model device. b) Real device printed in 3D®.

5.-Conclusions

This paper presents a methodology to accurately obtain and reproduce the 3D movement of the jaw in order to design customized MADs. The use of 2-D jaw models performs well in many cases. However, the proposed 3-D model yields to a more accurate description of the movement of both condyles. Consequently, it is possible to take into account asymmetries or malformations in the temporomandibular joints in the design stage of MADs.

This way, a 3D multibody model that reproduces the jaw movement has been described in this work. The movement of the human jaw has been studied and the appropriate movement restrictions of the jaw in the temporomandibular joint have been defined to obtain the 3D model. Thus, the movement of the lower incisor has been obtained by means of a vision system based on the use of infrared cameras and reflective markers. These data have made it possible to obtain the movement of the condyles.

Once the 3D model is developed, the movement of the jaw can be obtained when using a MAD. To this end, the desired trajectory of the lower incisor has to be previously defined. This trajectory is prescribed by a specialist to ensure the appropriate mandible advancement throughout its opening movement. This way, it is possible to accurately model the movement of the jaw and therefore obtain the trajectory of any other point attached to the mandible, such as the two followers of the MAD. Finally, the trajectories of the followers determine the design of the cams.

The development of a 3D model of the mandible makes it possible to obtain a more precise profile of the cam and its positioning in the splint. This is important since most patients do not have symmetrical jaws with respect to the sagittal plane. Therefore, a 3D study of the movement is necessary to ensure that the movement of the patient's jaw is natural and comfortable when using the device even if the patient suffers from problems in the temporomandibular joints. With this work, these problems can be detected and the design of the mandibular advancement device can be properly addressed. However, further works will be devoted to the study of MADs specifically designed for patients who suffer from serious problems in the temporomandibular

joints in which specialists report poor performance of current devices.

Author contributions

Conceptualization and methodology, M. García, J.A. Cabrera and A. Bataller; Investigation, all authors; Writing- Original Draft; J.A. Cabrera, A. Bataller and J.J. Castillo; Writing-Review & Editing, all authors.

Acknowledgements

A substantial part of the work described in this article was supported by the research contracts 806/31.4830 and 806/31.5511 between the private company Laboratorio Ortoplus S.L. and the University of Malaga, which is acknowledged with gratefulness.

Compliance with ethics guidelines

M. García, J.A. Cabrera, A. Bataller, S. Postigo and J.J. Castillo declare that they have no conflict of interest.

REFERENCES

[1] J.A. Dempsey, S.C. Veasey, B.J. Morgan, C.P. O'Donnell, Pathophysiology of sleep apnea, Phys. Rev. 90 (1) (2010) 47–112, doi: 10.1152/physrev.0 0 043.20 08 .

[2] A. Malhotra , D.P. White , Obstructive sleep apnoea, Lancet 360 (July 20) (2002) 238–245 .

[3] T. Douglas Bradley , J.S. Floras , Obstructive sleep apnoea and its cardiovascular consequences, Lancet 373 (January 3) (2009) 82–93 2009 .

[4] H. Wang, J.D. Newton, J.S. Floras, S. Mak, K.-L. Chiu, P. Ruttanaumpawan, G. Tomlinson, T. Douglas Bradley, Influence of obstructive sleep apnea on mortality in patients with heart failure, J. Am. Coll. Cardiol. 49 (15) (2007) ISSN 0735-1097/07. Published by Elsevier Inc., doi: 10.1016/j.jacc.2006.12.046 .

[5] H. Klar Yaggi , J. Concato , W.N. Kernan , J.H. Lichtman , L.M. Brass , V. Mohsenin , Obstructive sleep apnea as a risk factor for stroke and death, N. Engl. J. Med. 353 (November 10) (2005) 2034–2041 .

[6] L.J. Epstein , D. Kristo , J. Strollo Jr , N. Friedman , A. Malhotra , S.P. Patil , K. Ramar , R. Rogers , R.J. Schwab , E.M. Weaver , M.D. Weinstein , Clinical guideline for the evaluation, management and long-term care of obstructive sleep apnea in adults, J. Clin. Sleep Med. 5 (3) (2009) .

[7] K. Sutherland, et al. Oral appliance treatment for obstructive sleep apnea: An update. J. Clin. Sleep Med. 10, 215–227 (2014).

[8] P. Lloberes, et al. Diagnóstico y tratamiento del síndrome de apneas-hipopneas del sueño. Arch. Bronconeumol. (2011). doi:10.1016/j.arbres.2011.01.001

[9] P. Lloberes, et al. Fe de errores de 'Diagnóstico y tratamiento del síndrome de apneas-hipopneas del sueño'. Archivos de Bronconeumologia (2011). doi:10.1016/j.arbres.2011.04.001

[10] W. Bhat and Sr. Jayesh. Mandibular advancement device for obstructive sleep apnea: An overview. J. Pharm. Bioallied Sci. (2015). doi:10.4103/0975-7406.155915

[11] K. Sutherland, et al. Oral Appliance Treatment Response and Polysomnographic Phenotypes of Obstructive Sleep Apnea. J. Clin. Sleep Med. 11, 861–868 (2015).

[12] K. Sutherland, P.A. Cistullia, Mandibular advancement splints for the treatment of sleep apnea syndrome, Swiss Med. Weekly 141 (September) (2011) w13276, doi: 10.4414/smw.2011.13276 .

[13] M. Dieltjens, O.M. Vanderveken, P.H. Van de Heyning, M.J. Braem, Current opinions and clinical practice in the titration of oral appliances in the treatment of sleep-disordered breathing, Sleep Med. Rev. 16 (2012) 177–185, doi: 10.1016/j.smrv.2011.06.002 .

[14] W.L. Xu, J.E. Bronlund, J. Potgieter, K.D. Foster, O. Röhrle, A.J. Pullan, J.A. Kieser. Review of a human masticatory system and masticatory robotics. Mechanism and Machine Theory, vol. 43, pp. 1353-1375 (2008).

[15] B. Daumas, W.L. Xu, J. Bronlund. Jaw mechanism modeling and simulation. Mechanism and Machine Theory, vol. 40, pp. 821-833, (2005).

[16] H. Takanobu, A. Takanishi, D. Ozawa, K. Ohtsuki, M. Ohnishi, A. Okino. Integrated dental robot system for mouth opening and closing training. Proceeding of the 2002 IEEE International Conference on Robotics & Automation, (2002).

[17] S.J. Lee, B.K. Kim, Y.G. Chun, D.J. Park. Design of mastication robot with life-sized linear actuator of human muscle and load cells for measuring force distribution on teeth. Mechatronics, vol. 51, pp. 127-136, (2018).

[18] W.L. Xu, J.S. Pap and J. Bronlund. Design of a biologically inspired parallel robot for foods chewing. IEEE Transactions on Industrial Electronics, vol. 55, pp. 832-841, (2008).

[19] M. J. Delsignore, V. N. Krovi. Screw-theoretic analysis models for felid jaw mechanisms. Mechanism and Machine Theory, vol. 43, pp. 147-159, (2008).

[20] U. Posselt. Studies in the mobility of the human mandible. Acta Scandinavica. (1952).

[21] F. Yuan, H. Sui, Z. Li, H. Yang, P. Lu, Y. Wang, Y. Sun. A method of three-dimensional recording of mandibular movement based on two-dimensional image feature extraction. PloS ONE, vol. 10, (2015).

[22] J.J Fang, T.H. Kuo. Modelling of mandibular movement. Computers in Biology and Medicine, vol. 38, pp. 1152-1162, (2008).

[23] R. Enciso, A. Memon, D. A. Fidaleo, U. Neumann, J. Mah. The virtual craniofacial patient: 3D jaw modeling and animation. Studies in health technology and informatics, vol. 94, pp. 65-71, (2003).

[24] A.P. Pinheiro, A.A. Pereira, A.O. Andrade, D. Bellomo. Measurement of jaw motion: the proposal of a simple and accurate method. Journal of Medical Engineering & Techonology, vol. 35, pp. 125-133, (2011).

[25] A. Bataller, J.A. Cabrera, M. García, J.J. Castillo, P. Mayoral. Cam synthesis applied to the design of a customized mandibular advancement device for the treatment of obstructive sleep apnea. Mechanism and Machine Theory, vol. 123, pp. 153-165 (2018).

[26] J. García de Jalón, E. Bayo. Kinematic and dynamic simulation of multibody systems. Springer-Verlag New York (1994).